Boundary Control of Open Channels With Numerical and Experimental Validations

Valérie Dos Santos and Christophe Prieur

***Abstract*—The problem of the stabilization of the flow in a reach is investigated. To study this problem, we consider the nonlinear Saint-Venant equations, written as a system of two conservation laws perturbed by non-homogeneous terms. The non-homogeneous terms are due to the effects of the bottom slope, the slope's friction, and also the lateral supply. The boundary actions are defined as the position of both spillways located at the extremities of the reach. It is assumed that the height of the flow is measured at both extremities. Assuming that the non-homogeneous terms are sufficiently small in C^1-norm, we design stabilizing boundary output feedback controllers, i.e., we derive a new strategy which depends only on the output and which ensures that the water level and water flow converge to the equilibrium. Moreover, the speed of the convergence is shown to be exponential. The proof of this result is based on the estimation of the effects on the non-homogeneous terms on the evolution of the Riemann coordinates. This stability result is validated both by simulating on a real river data and by experimenting on a micro-channel setup.**

***Index Terms*—Asymptotic stability, nonlinear systems, partial differential equations (PDEs), flow control.**

I. Introduction

IRRIGATION channel's regulation problem presents an economic and environmental interest and much research is done in this area. Indeed, water losses in open channels, due to inefficient management and control, may be large. To avoid overflows and satisfy water demand, the level of instrumentation (e.g., water level measurements and operating motor-driven gates) and automation in open channel networks increases (see [15] for an overview).

In order to deliver water, it is important to ensure that the water level and the flow rate in the open channel remain at certain values. The difficulty of this control system is that only the gates positions are able to meet performance specifications. This asks to design boundary control laws satisfying the control objectives.

This problem has been previously considered in the literature using a wide variety of techniques. See the use of classical linear control theory in [14], [17], and [19]. Some of them take into account the uncertainties and apply robust control approach (see, e.g., [11]–[13]). Studying directly the nonlinear dynamics is also possible as in [5] and [20]. In [10], the Saint-Venant equations are linearized and, using a numerical method, the authors succeed to compute the frequency response of the linear system, and to use this approach on an irrigation channel. Here, we consider the nonlinear Saint-Venant equations and we derive a new theoretical result to take the nonhomogeneous terms into account when designing stabilizing boundary output feedback controllers. Moreover, we illustrate our main result on numerical simulations and on real experiments.

Recent approaches consider the distributed feature of the system. Using the Riemann coordinates approach on the Saint-Venant equations, stability results are given in [7] for a system of two conservation laws, and in [9] for system of larger dimension. Lyapunov techniques have been used in [2] and [4].

In this paper, we consider the nonlinear Saint-Venant equations and we take the friction and the slope into account. Also, some additional flows (as rain, or water loss) are modelled. These terms make the model nonhomogeneous, and should be considered when designing the boundary actions. We get a system of two conservation laws, that are described by hyperbolic partial differential equations, with one independent time variable $t \in [0, \infty)$ and one independent space variable on a finite interval $x \in [0, L]$. This system is perturbed by nonhomogeneous terms when modelling the friction, the slope, and the additional supply rate. The considered problem is the design of feedback control actions (the gates) at the boundaries (i.e., at $x = 0$ and $x = L$) in order to ensure that the smooth solution of the Cauchy problem exists and converges to a desired steady state. We assumed that we measure the water level at each boundary, and we succeed to use this output only when designing our stabilizing boundary feedback.

Recently, the theoretical problem of the stability of a system of two conservation laws perturbed by nonhomogeneous terms has been first investigated in [18]. Here, we make the sufficient condition for the asymptotic stability more quantitative, we explicit a condition on the size of the nonhomogeneous terms, and we compute some stabilizing boundary output feedback controllers for the perturbed Saint-Venant equations. The computation of this sufficient condition is based on estimations of the Riemann coordinates along the characteristic curves. Moreover, this new stability result is illustrated with numerical simulations using the data of a real river (namely the Sambre in Belgium), and experimentations on a micro-channel (more precisely the Valence experimental reach).

This paper can be seen as a generalization of [8], where Saint-Venant equations without nonhomogeneous terms are considered. Moreover, in this paper, we illustrate our main result on experiments (and not only on numerical simulations as in [8]).

Manuscript received March 14, 2007; revised October 3, 2007. Manuscript received in final form January 31, 2008. First published June 10, 2008; current version published October 22, 2008. Recommended by Associate Editor M. de Mathelin. This work was supported by the IEEE.

V. Dos Santos is with Université de Lyon, Lyon F-69003, France, and Université Lyon 1, CNRS, UMR 5007, LAGEP, Villeurbanne, F-69622, France (e-mail: dossantos@lagep.cpe.fr).

C. Prieur is with LAAS-CNRS, Université de Toulouse, 31077 Toulouse, Cedex 4, France (e-mail: christophe.prieur@laas.fr).

Color versions of one or more of the figures in this paper are available online at http://ieeexplore.ieee.org.

Digital Object Identifier 10.1109/TCST.2008.919418

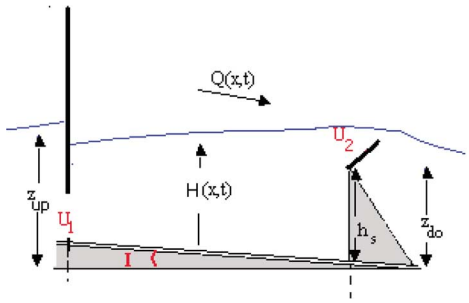

Fig. 1. Scheme of a channel: One reach with an overflow gate.

This paper is organized as follows. After a short presentation of the Saint-Venant equations (see Section II), the problem is stated, the tools presented, and the stability result established in Section III. In Section IV, simulations results are produced on the Sambre and, in Section V, we illustrate our main result by means of experiments of a pilot channel. Section VI contains some concluding remarks and our stability result is proven in the Appendix.

II. Description of the Model and Statement of the Problem

A. Saint-Venant Equations

We consider a reach of an open channel as represented in Fig. 1.

We assume that the channel is prismatic with a constant rectangular section. Note that in our configuration, the slope could be non-null as well as the friction effects.

In the field of hydraulics, the flow in open channel is generally stated by the so-called Saint-Venant equations, namely a law of mass conservation and a law of momentum conservation (see [6], e.g.)

$$\partial_t H + \partial_x(Q/B) = q \tag{1}$$

$$\partial_t Q + \partial_x\left(\frac{Q^2}{BH} + \frac{1}{2}gBH^2\right) = gBH(I-J) + kq\frac{Q}{BH} \tag{2}$$

where $H(t,x)$ stands for the water level and $Q(t,x)$ the water flows in the reach while g denotes the gravitation constant $(m.s^{-2})$. In the previous, $x \mapsto I(x)$ is the bottom slope function $(m.m^{-1})$, B is the channel width (m), and J is the slope's friction $(m.m^{-1})$. The function $(x,t) \mapsto q(x,t)$ stands for a lateral flow by unit length $(m^2.s^{-1})$. We assume that this function is continuously differentiable and $q > 0 (k = 0)$ for supply (rain), negative $(k = 1)$ for loss (evaporation). We emphasize that the function q should be continuously differentiable. However, by approximating any discontinuous functions by a continuously differentiable function, we may also consider localized withdrawals, i.e., we may approximate discontinuous lateral flows.

The slope's friction J is expressed with the following Manning–Strickler expression

$$J(Q,H) = \frac{n_M^2 Q^2}{S(H)^2 R(H)^{4/3}}$$

where n_M is the Manning coefficient $(s.m^{-1/3})$, $S(H) = BH$ is the wet perimeter (m), and $R(H) = (BH/B + 2H)$ is the hydraulic radius (m).

The system is rewritten as follows:

$$\partial_t \begin{pmatrix} H \\ Q \end{pmatrix} + A(H,Q)\partial_x \begin{pmatrix} H \\ Q \end{pmatrix} = h(H,Q) \tag{3}$$

with the matrices $A(H,Q)$ and $h(H,Q)$ defined as

$$A(H,Q) = \begin{pmatrix} 0 & 1/B \\ -\frac{Q^2}{BH^2} + gBH & \frac{2Q}{BH} \end{pmatrix}$$

$$h(H,Q) = \begin{pmatrix} q \\ gBH(I-J) + kq\frac{Q}{BH} \end{pmatrix}. \tag{4}$$

The control actions are the positions U_0 and U_L of both spillways located at the extremities of the pool and related to the state variables H and Q by the following expressions. In this paper, the gates at $x = 0$ and $x = L$ are, respectively:

- a submerged underflow gate

$$Q(0,t) = U_0 B \mu_0 \sqrt{2g(z_{\text{up}} - H(0,t))} \tag{5}$$

  where z_{up} is the water level before the gate;
- a submerged overflow gate

$$H(L,t) = \left(\frac{Q^2(L,t)}{2gB^2\mu_L^2}\right)^{1/3} + h_s + U_L \tag{6}$$

  where z_{do} is the water level after the gate and h_s is the height of the fixed part of the overflow gate (see Fig. 1). The water flow coefficient of the ith gate is denoted μ_i.

Other kinds of boundary conditions (BCs) can be considered, e.g., two submerged underflow gates (or two submerged overflow gates) at $x = 0$ and at $x = L$.

B. Problem Under Consideration

In order to introduce the problem under consideration in this paper, we need some additional notations.

- The usual Euclidean norm $|\cdot|$ in $\mathbb{R}$ is denoted by $|\cdot|$. The ball centered in $0 \in \mathbb{R}$ with radius $\varepsilon > 0$ is denoted $B(\varepsilon)$.
- Given Φ continuous on $[0,L]$ and Ψ continuously differentiable on $[0,L]$, we denote

$$|\Phi|_{C^0(0,L)} = \max_{x\in[0,L]}|\Phi(x)|$$
$$|\Psi|_{C^1(0,L)} = |\Psi|_{C^0(0,L)} + |\Psi'|_{C^0(0,L)}.$$

- The set of continuously differentiable functions $\Psi^{\#} : [0,L] \to \mathbb{R}$ satisfying the compatibility assumption $\mathcal{C}$ and $|\Psi^{\#}|_{C^1(0,L)} \le \varepsilon$ is denoted $B_{\mathcal{C}}(\varepsilon)$.

For constant control actions $U_0(t) = \bar{U}_0$ and $U_L(t) = \bar{U}_L$, a *steady-state solution* is a constant solution $(H,Q)(t,x) = (\bar{H},\bar{Q})(x)$, for all $t \in [0,+\infty)$, for all $x \in [0,L]$, which satisfies (3) and the BCs (5) and (6).

At time $t \ge 0$, *the output* of the system (3) is given by $y(t) = (H_0(t), H_L(t))$.

The problem under consideration in this work is as follows.

Problem 1: Given a steady-state $(\bar{H},\bar{Q})$, called the set point, we consider the problem of the local exponential stabilization of (3) by means of a boundary output feedback controller, i.e., we want to compute a boundary output feedback controller

$y \mapsto (U_0(y), U_L(y))$ such that, for any smooth small enough (in C^1-norm) initial condition $H^\#$ and $Q^\#$ satisfying some compatibility conditions, the partial differential equation (PDE) (3) with the BCs (5) and (6) and the initial condition

$$(H,Q)(x,0) = (H^\#, Q^\#)(x) \forall x \in [0,L] \tag{7}$$

has a unique smooth solution converging exponentially fast (in C^1-norm) towards $(\bar{H}, \bar{Q})$.

III. Stability Result

First, note that the system (3) is strictly hyperbolic, i.e., the Jacobian matrix of $A(H,Q)$, defined by (4), has two non-zero real distinct eigenvalues

$$\lambda_1(H,Q) = \frac{Q}{BH} + \sqrt{gH}$$
$$\lambda_2(H,Q) = \frac{Q}{BH} - \sqrt{gH}. \tag{8}$$

They are generally called *characteristic velocities*.

The flow is said to be *fluvial* (or subcritical) when the characteristic velocities have opposite signs

$$\lambda_2(H,Q) < 0 < \lambda_1(H,Q).$$

Under constant BCs $Q(0,t) = \bar{Q}_0$ and $H(L,t) = \bar{H}_L$, for all t, there exists a steady-state solution $x \mapsto (\bar{H}, \bar{Q})$ satisfying

$$\partial_x \bar{H}(x) = -g\bar{H}\frac{I - \bar{J}}{\bar{\lambda}_1 \bar{\lambda}_2} - q\frac{\bar{Q}}{B^2\bar{H}}\frac{(k-2B)}{\bar{\lambda}_1\bar{\lambda}_2}$$
$$\partial_x \bar{Q}(x) = Bq \tag{9}$$

with $\bar{\lambda}_1 = \lambda_1(\bar{H}, \bar{Q})$ and $\bar{\lambda}_2 = \lambda_2(\bar{H}, \bar{Q})$.

Let t_1 be the time instant defined by

$$x_1(t_1) = L \tag{10}$$

where x_1 is the solution of the Cauchy problem $\dot{x}_1(t) = \lambda_1(\bar{H}, \bar{Q}), x_1(0) = 0$. Similarly, let t_2 be the time instant defined by

$$x_2(t_2) = 0 \tag{11}$$

where x_2 is the solution of the Cauchy problem $\dot{x}_2(t) = \lambda_2(\bar{H}, \bar{Q}), x_2(L) = 0$.

To state our stability result, we need to introduce the notations found in (12)–(14), shown at the bottom of the page. We are now in position to state our main result.

Theorem: Let t_1, t_2, ℓ_1 and ℓ_2 be defined by (10), (11), (13), and (14), respectively.

If the bottom slope function I, the slope's friction function J, and the lateral flow function q are sufficiently small in C^1 norm, then we have

$$\max(t_1\ell_1, t_2\ell_2) < 1. \tag{15}$$

In that case, for all $(k_0, k_L) \in \mathbb{R}^2$ such that

$$|k_0 k_L| + t_2|k_0|\ell_2 + t_1\ell_1 < 1 \tag{16}$$
$$|k_0 k_L| + t_1|k_L|\ell_1 + t_2\ell_2 < 1 \tag{17}$$

$$\bar{a} = \left(\frac{\bar{Q}}{B\bar{H}} + 2\sqrt{g\bar{H}}\right), \quad \bar{b} = \left(\frac{\bar{Q}}{B\bar{H}} - 2\sqrt{g\bar{H}}\right) \tag{12}$$

$$\ell_1 = \max\left(\frac{g}{\bar{\lambda}_1}\left\{\frac{3I}{4} + \frac{n_M^2}{16B^{4/3}} \times \left[(3\bar{a}-\bar{b})(\bar{a}+\bar{b})\left(2 + \frac{16Bg}{(\bar{a}-\bar{b})^2}\right)^{4/3} - \frac{8}{3}16Bg\frac{(3\bar{a}+\bar{b})(\bar{a}+\bar{b})^2}{(\bar{a}-\bar{b})^3} \times \left(2 + \frac{16Bg}{(\bar{a}-\bar{b})^2}\right)^{1/3}\right]\right\}\right.$$
$$+ \frac{q}{\bar{\lambda}_1}\frac{g}{B}\left[-2\frac{(3\bar{a}+\bar{b})}{(\bar{a}-\bar{b})^3} \times \left(\frac{k}{2}(\bar{a}+\bar{b}) - \frac{B}{4}(\bar{a}+3\bar{b})\right) + \frac{(3\bar{a}+\bar{b})}{(\bar{a}-\bar{b})^2}\left(\frac{k}{2} - \frac{B}{4}\right) - \frac{3}{(\bar{a}-\bar{b})^2} \times \left(\frac{k}{2}(\bar{a}+\bar{b}) - \frac{B}{4}(\bar{a}+3\bar{b})\right)\right],$$
$$\frac{g}{\bar{\lambda}_1}\left\{\frac{I}{4} + \frac{n_M^2}{16B^{4/3}} \times \left[(5\bar{a}+\bar{b})(\bar{a}+\bar{b})\left(2 + \frac{16Bg}{(\bar{a}-\bar{b})^2}\right)^{4/3} + \frac{8}{3}16Bg\frac{(3\bar{a}+\bar{b})(\bar{a}+\bar{b})^2}{(\bar{a}-\bar{b})^3} \times \left(2 + \frac{16Bg}{(\bar{a}-\bar{b})^2}\right)^{1/3}\right]\right\}$$
$$\left. + \frac{q}{\bar{\lambda}_1}\frac{g}{B}\left[2\frac{(3\bar{a}+\bar{b})}{(\bar{a}-\bar{b})^3}\left(\frac{k}{2}(\bar{a}+\bar{b}) - \frac{B}{4}(\bar{a}+3\bar{b})\right) + \frac{(3\bar{a}+\bar{b})}{(\bar{a}-\bar{b})^2}\left(\frac{k}{2} - 3\frac{B}{4}\right) - \frac{1}{(\bar{a}-\bar{b})^2}\left(\frac{k}{2}(\bar{a}+\bar{b}) - \frac{B}{4}(\bar{a}+3\bar{b})\right)\right]\right) \tag{13}$$

$$\ell_2 = \max\left(\frac{g}{\bar{\lambda}_2}\left\{\frac{I}{4} + \frac{n_M^2}{16B^{4/3}} \times \left[(\bar{a}+5\bar{b})(\bar{a}+\bar{b})\left(2 + \frac{16Bg}{(\bar{a}-\bar{b})^2}\right)^{4/3} - \frac{8}{3}16Bg\frac{(\bar{a}+3\bar{b})(\bar{a}+\bar{b})^2}{(\bar{a}-\bar{b})^3} \times \left(2 + \frac{16Bg}{(\bar{a}-\bar{b})^2}\right)^{1/3}\right]\right.\right.$$
$$\left. + \frac{q}{B}\left[-2\frac{(\bar{a}+3\bar{b})}{(\bar{a}-\bar{b})^3}\left(\frac{k}{2}(\bar{a}+\bar{b}) - \frac{B}{4}(3\bar{a}+\bar{b})\right) + \frac{(\bar{a}+3\bar{b})}{(\bar{a}-\bar{b})^2}\left(\frac{k}{2} - 3\frac{B}{4}\right) - \frac{1}{(\bar{a}-\bar{b})^2}\left(\frac{k}{2}(\bar{a}+\bar{b}) - \frac{B}{4}(3\bar{a}+\bar{b})\right)\right]\right\},$$
$$\frac{g}{\bar{\lambda}_2}\left\{\frac{3I}{4} + \frac{n_M^2}{16B^{4/3}}\left[-(\bar{a}-3\bar{b})(\bar{a}+\bar{b}) \times \left(2 + \frac{16Bg}{(\bar{a}-\bar{b})^2}\right)^{4/3} + \frac{8}{3}16Bg\frac{(\bar{a}+3\bar{b})(\bar{a}+\bar{b})^2}{(\bar{a}-\bar{b})^3} \times \left(2 + \frac{16Bg}{(\bar{a}-\bar{b})^2}\right)^{1/3}\right]\right.$$
$$\left.\left. + \frac{q}{B}\left[2\frac{(\bar{a}+3\bar{b})}{(\bar{a}-\bar{b})^3}\left(\frac{k}{2}(\bar{a}+\bar{b}) - \frac{B}{4}(3\bar{a}+\bar{b})\right) + \frac{(\bar{a}+3\bar{b})}{(\bar{a}-\bar{b})^2}\left(\frac{k}{2} - \frac{B}{4}\right) - \frac{3}{(\bar{a}-\bar{b})^2}\left(\frac{k}{2}(\bar{a}+\bar{b}) - \frac{B}{4}(3\bar{a}+\bar{b})\right)\right]\right\}\right) \tag{14}$$

the following boundary output feedback controller:

$$U_0 = H_0 \frac{\frac{\bar{Q}_0}{B\bar{H}_0} - 2\sqrt{g}\alpha_0(\sqrt{H_0} - \sqrt{\bar{H}_0})}{\mu_0\sqrt{2g(z_{\text{up}} - H(0,t))}} \tag{18}$$

$$U_L = H_L - h_s - \left[\frac{\left(H_L\left[\frac{\bar{Q}_L}{B\bar{H}_L} + 2\sqrt{g}\alpha_L(\sqrt{H_L} - \sqrt{\bar{H}_L})\right]\right)^2}{2g\mu_L^2}\right]^{1/3} \tag{19}$$

where $H_0 = H(t,0), H_L = H(t,L), \alpha_0 = (1-k_0)/(1+k_0)$, and $\alpha_L = (1-k_L)/(1+k_L)$ makes the closed-loop system locally exponentially stable, i.e., there exist $\varepsilon > 0, C > 0$, and $\mu > 0$ such that, for all bottom slope functions I, slope's friction functions J, and lateral flow functions q sufficiently small in C^1 norm, for all initial conditions $(H^\#, Q^\#) : [0,L] \to (0,+\infty)$ continuously differentiable, satisfying the compatibility conditions, shown in (20) and (21) at the bottom of the page, and the inequality

$$|(H^\#, Q^\#) - (\bar{H}, \bar{Q})|_{\mathcal{C}^1(0,L)} \leq \varepsilon$$

there exists a unique C^1 solution of the Saint-Venant equations (3), with the BCs (5) and (6), and the initial condition (7), defined for all $(x,t) \in [0,L]\times[0,+\infty)$. Moreover, it satisfies, for all $t \geq 0$

$$|(H,Q)(.,t) - (\bar{H},\bar{Q})|_{C^1(0,L)} \leq C_1 e^{-\mu t}|(H^\#, Q^\#)|_{C^1(0,L)}. \tag{22}$$

Remark 1: Some observations are in order.

- The compatibility conditions (20) and (21) are obtained by time differentiation of the BCs (5) and (6) and using (18) and (19).
- This result states that the speed of convergence is exponential. It is also possible to estimate how large is the speed by estimating the positive number μ in (22). Indeed, we prove that the value μ is a decreasing function of the product $|k_0 k_L|$. Thus, to increase the speed of convergence, it is needed to decrease the value of $|k_0 k_L|$. See Remark 2 for a proof of this remark and Section IV for an illustration by simulating on a real river and by experimenting on a micro-channel.

TABLE I
PARAMETERS OF A REACH OF THE SAMBRE RIVER

parameters	B (m)	L (m)	slope I $(m^1.m^{-1})$	μ_0 $= \mu_L$	K $(m^{1/3}.s^{-1})$
values	40	11239	$7.92e^{-5}$	0.4	33

Fig. 2. Picture of the Sambre River.

We postpone the proof of this result in the Appendix.

In the following sections, we apply our stability result on numerical simulations of a river and on an experimental setup. In both cases, the assumption (15) is satisfied, thus, we succeed to design a stabilizing boundary output feedback controller. Let us note that if the inequalities (16) and (17) hold, then we have

$$|k_0 k_L| < \min(1 - t_1\ell_1, 1 - t_2\ell_2). \tag{23}$$

IV. NUMERICAL SIMULATIONS ON THE SAMBRE RIVER

To illustrate our result, simulations have been realized with the realistic data of the Sambre River located in Belgium. Physical parameters of this river are given in Table I and the gates are overflow ones (see Fig. 2).

For the regulation of the Sambre, a proportional–integral differential (PID) controller is actually used on site. The advantage of our output feedback controller is to allow a greater variation of the water height and flow and not to be restricted only around an initial equilibrium as it is the case for linearized approach (as those considered in [10], [17], [19], and among other references).

$$gBH^\#(0)(I-J(0)) + kq(0)\frac{Q^\#(0)}{BH^\#(0)} - \frac{d}{dx}\left(\frac{Q^2}{BH^\#} + \frac{1}{2}gBH^{\#}2\right)(0)$$
$$= \left(q - \frac{d}{dx}\frac{Q^\#}{B}\right)(0)B \times \left[\frac{\bar{Q}(0)}{B\bar{H}(0)} + 2\alpha_0\sqrt{g\bar{H}} - 3\alpha_0\sqrt{gH(0)}\right] \tag{20}$$

$$gBH^\#(L)(I - J(L)) + kq(L)\frac{Q^\#(L)}{BH^\#(L)} - \frac{d}{dx}\left(\frac{Q^2}{BH^\#} + \frac{1}{2}gBH^{\#}2\right)(L)$$
$$= \left(q - \frac{d}{dx}\frac{Q^\#}{B}\right)(L)B \times \left[\frac{\bar{Q}(L)}{B\bar{H}(L)} - 2\alpha_L\sqrt{g\bar{H}(L)} + 3\alpha_l\sqrt{gH(L)}\right] \tag{21}$$

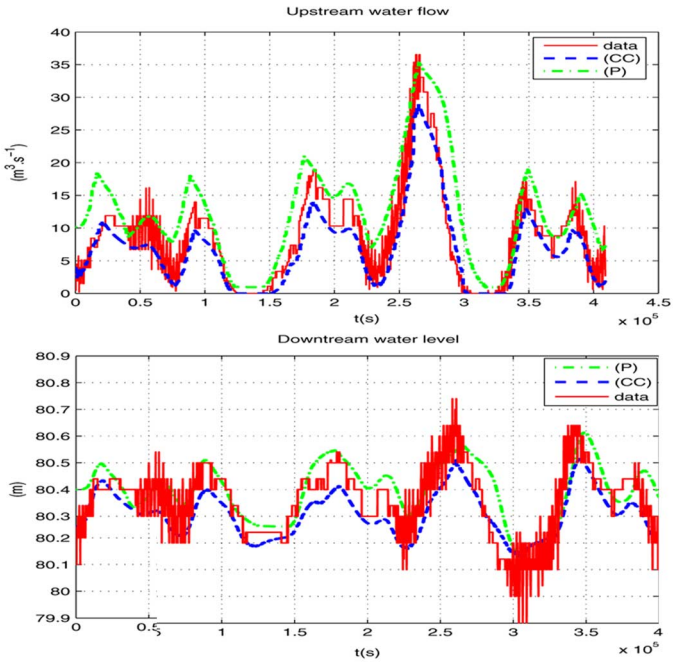

Fig. 3. Water flow and water level at (left) $x = 0$ and at (right) $x = L$ using either the Preismann scheme, or the Chang and Cooper scheme, or the real data.

A. Description of the Numerical Scheme

For all numerical simulations, we use the Chang and Cooper theta-scheme of order 2 [1]. To validate this numerical discretization, we compare the numerical simulations with real data and with numerical simulations using the Preismann scheme (which is used in other works dealing with the control of flows [12], [16]). Consider Fig. 3, where we may compare the upstream water flow and the downstream water flow, on the reach number 2 using the following:

(P) Preismann scheme for which the initial conditions are the theoretical ones;

(CC) Chang and Cooper scheme for which the initial conditions (IC) are the measured ones;

(data) real data measured on the Sambre River.

We check that the Chang and Cooper scheme gives a numerical solution which is close to the real one and has a more realistic dynamic than the Preismann scheme. The simulations have been realized with MATLAB and Simulink.

B. Simulation Results

For an initial condition satisfying our compatibility conditions, we choose $Q^{\#}(0) = 10\ \mathrm{m}^3 \cdot s^{-1}, H^{\#}(0) = 3.75$ m, $H^{\#}(L) = 4.65$ m.

In these numerical simulations, we consider the stability problem around the following equilibrium computed with (9) and $\bar{Q} = 12\ \mathrm{m}^3 \cdot \mathrm{s}^{-1}, \bar{H}(0) = 3.80$ m, $\bar{H}(L) = 4.7$ m. Using (8), we compute the eigenvalues $\lambda_1 \approx 6\ \mathrm{m} \cdot \mathrm{s}^{-1}$ and $\lambda_2 \approx -6\ \mathrm{m} \cdot \mathrm{s}^{-1}$. Thus, the flow is fluvial.

Times instants t_1 and t_2 are computed with (10) and (11), and they take the following values $t_1 = 18\,294.10^3$ s and $t_2 = 18\,723.10^3$ s. Using (23), we note that the tuning parameters should satisfy $|k_0 k_L| \leq 0.65$.

To illustrate Theorem 1, three simulations have been computed with the following values.

(S1) $k_0 = -0.2520$ and $k_L = -0.1632$, (we compute $k_0 k_L = 0.041$). The stability condition (16) and (17) is satisfied, and thus, the inequality (23) is satisfied. We check on the evolution of the water, that the level and the flow converge to the equilibrium.

(S2) $k_0 = -0.9199$ and $k_L = -0.5956$, (we compute $k_0 k_L = 0.55$). Condition (17) is satisfied, whereas (16) does not hold. However, we observe that the level and the flow of the water converge to the equilibrium. With this simulation, we check that the condition (16) and (17) is sufficient for the stability but is not necessary.

(S3) $k_0 = -1.05$ and $k_L = -0.68$, the stability condition (16) and (17) is not satisfied and the level and the flow of the water do not converge to the equilibrium. This implies that the stability is not ensured for all boundary control actions.

See the evolutions of the level at $x = L$ and the flow at $x = 0$ of the water in Fig. 4 for these three numerical simulations. At the top, the evolution of the water flow at $x = 0$ and the water level at $x = L$ is depicted for each numerical experiment, and at down the evolution of the gates at upstream and downstream of the reach.

These simulations confirm that the stability condition (16) and (17) is sufficient but not necessary for the stability. Moreover, let us note that we have considered an initial condition which is close to the equilibrium point since we have only a local asymptotic stability property and not a global one, as claimed in Theorem 1.

Moreover, it illustrates Remark 1, since we can check that the smaller is the product $|k_0 k_L|$, the higher is the speed of convergence. But the overshoot growths up also and a compromise should be done between the speed of convergence and the maximum overshoot admissible.

To cancel the offset on simulations (S1) and (S2), we add an integral action to the Riemann controller. The stability has been proved for the linearized Saint-Venant equations in [4]. Such result has not yet been extended for the nonlinear Saint-Venant (1), but we check in Section IV-D that adding a small integral may cancel the offset on the numerical simulations.

C. Open-Loop Comparison in the Simulations

In this section, we check that the convergence speed of the closed-loop system is greater than the one of the open-loop system. Considering the equilibrium and the initial condition of Section IV-B, we compare in Fig. 5, the numerical simulations of the open-loop system (S1OL) and the closed-loop system (S1CL) using the parameters of the simulation (S1) [thus, (S1) is equivalent with (S1CL)]. We check that the system in closed loop with our controller converges faster to the equilibrium than

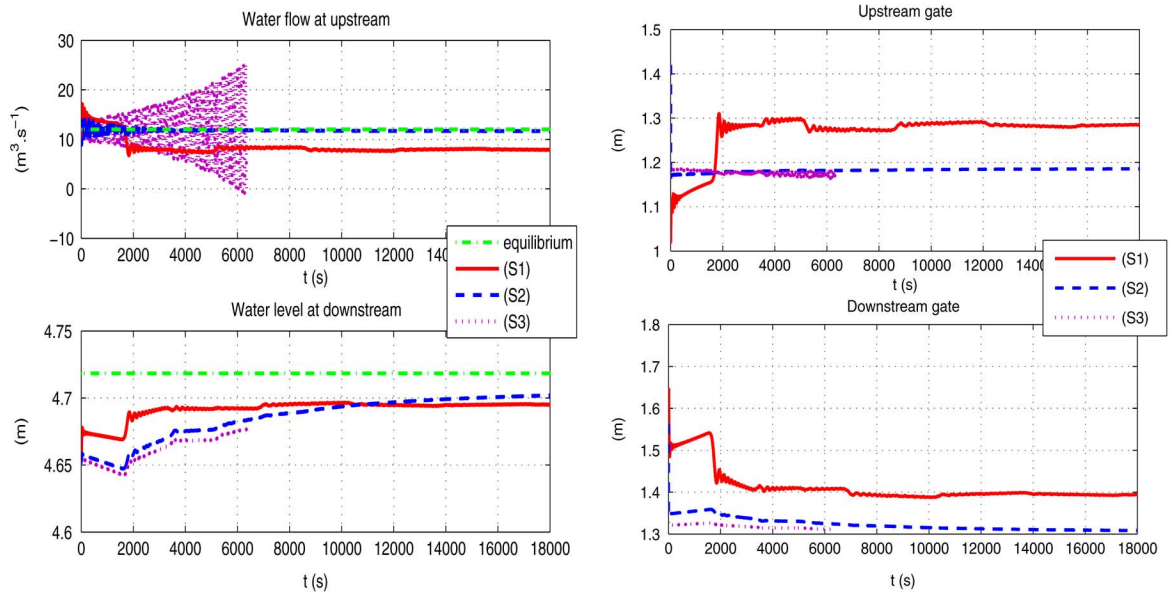

Fig. 4. Water flow at $x = 0$ and water level at (left) $x = L$, and level of the gates at $x = 0$ and (right) $x = L$ for the three numerical simulations (S1)–(S3).

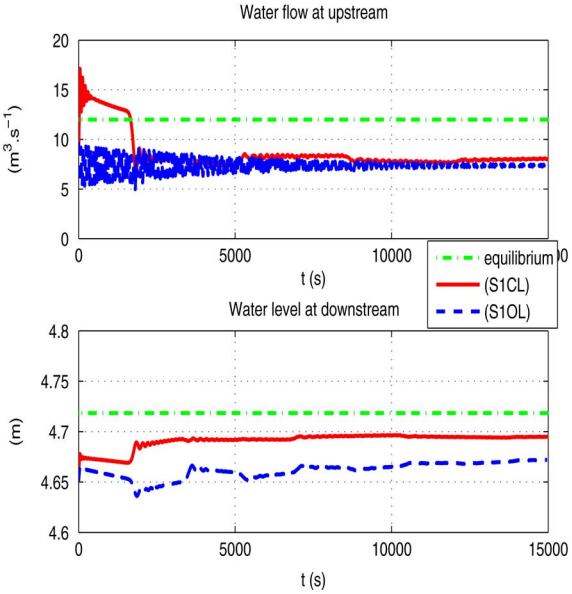

Fig. 5. Water flow at $x = 0$ and water level at $x = L$ for the simulation (S1) in open (S1OL) and closed (S1CL) loop.

the open-loop system. This comparison allows us to exhibit the value of the feedback.

D. Adding an Integral Action in the Simulations

In this section, we check on numerical simulations that adding an integral action on the controller given by Theorem 1 may cancel the offset. To this end, we consider the boundary control laws U_0 and U_L given by (18) and (19), respectively, and we add the integrals $m_0 \int_0^t Q(0,s)\,\mathrm{ds}$ and $m_L \int_0^t H(L,s)\,\mathrm{ds}$, respectively, where m_0, m_L are additional constant design parameters that have to be tuned.

We choose the same initial condition and the same equilibrium as in Section IV-B.

Two simulations (see Fig. 6) have been computed with the following values.

(SI1) For k_0 and k_L, we choose the same values as for (S1), whereas we choose for the parameters of the integral action $m_0 = 0.005$ and $m_L = -0.005$. It allows to cancel the offset appearing with (S1).

(SI2) For k_0 and k_L, we choose the same values as for (S2), whereas we choose for the parameters of the integral action $m_0 = 0.005$ and $m_L = -0.005$. The system converges towards the equilibrium required in spite of some oscillations.

The parameters m_0 and m_L should be chosen carefully to satisfy the constraints of the system (for example, the size of the overshot). However, the integral correction succeeds to cancel the offset. The theoretical way to tune this set of parameters is a topic of further research, beyond the scope of this paper dealing with the nonlinear system (3). The linear case has been studied recently in [4].

V. Experimental Results on a Pilot Channel

An experimental validation has been performed on the Valence micro-channel (see Figs. 7 and 8, and the physical parameters in Table II). This pilot channel is located at ESISAR[1]/INPG[2] Engineering School in Valence, France. It is operated under the responsibility of the LCIS[3] Laboratory. This experimental channel (total length = 8 m) has an adjustable slope and a rectangular cross-section (width = 0.1 m). The channel is ended at downstream by a variable overflow spillway and equipped with three underflow control gates (see Figs. 7 and 8). Ultrasound sensors provide water level measurements at different locations

[1]École Supérieure d'Ingénieurs en Systèmes industriels Avancés Rhône-Alpes

[2]Institut National Polytechnique de Grenoble

[3]Laboratoire de Conception et d'Intégration des Systèmes

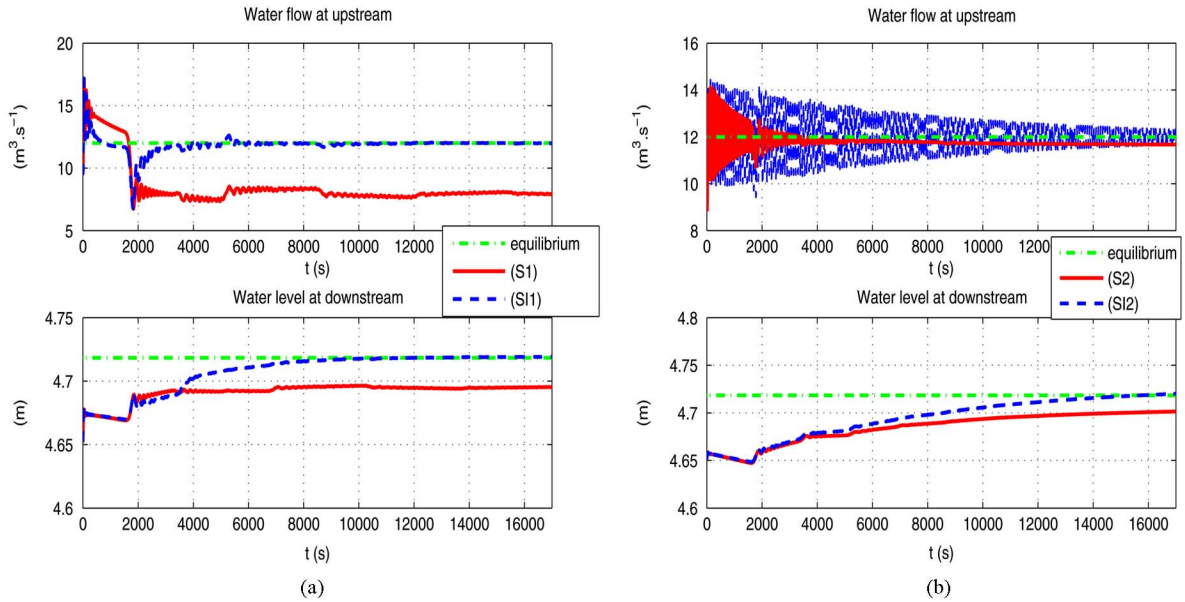

Fig. 6. Comparison of the water flow at $x = 0$ and water level at $x = L$ between the simulations with and without integral controller. (a) (S1) and (SI1). (b) (S2) and (SI2).

Fig. 7. Pilot channel of Valence.

of the channel (see Fig. 9). Note that water flow is deduced from the gate equations and has not been measured directly.

The aim of this section is to illustrate our main result on this pilot channel. Note that other techniques have been successfully applied on micro-channels (see, e.g., [16]). The main advantages of our approach is that we avoid any linearization of our PDE model and we get an exponential asymptotic stability.

The data pictured in the following has been filtered to get a better idea of the experimentation results. One reach has a length of 70 dm, the water level at upstream of the first gate is $z_{\rm up} = 1.72$ dm and at downstream of the second gate $z_{\rm do} = 0.85$ dm (theoretical values).

A. *Experimental Results*

The initial condition satisfies the compatibility conditions and $Q^{\#}(0) = 2.5\ \mathrm{dm}^3 \cdot \mathrm{s}^{-1}, H^{\#}(0) = 1.1$ dm, and $H^{\#}(L) = 1.25$ dm, whereas the equilibrium satisfies $\bar{Q}(0) = 2\ \mathrm{dm}^3 \cdot \mathrm{s}^{-1}, \bar{H}(0) = 1.3$ dm, and $\bar{H}(L) = 1.43$ dm. Using (8), we compute the eigenvalues $\lambda_1 \approx 13\ \mathrm{m} \cdot \mathrm{s}^{-1}$ and $\lambda_2 \approx -10\ \mathrm{m} \cdot \mathrm{s}^{-1}$. Thus, the flow is fluvial.

To illustrate Theorem 1, three experiments have been done. The results are pictured in Fig. 10, with $\max k_0 k_L = 0.90$ and the following values:

(E1) $k_0 = -0.0853, k_L = -0.463$ (we compute $k_0 k_L = 0.0395$);

(E2) $k_0 = -0.2134, k_L = -1.1575$ (we compute $k_0 k_L = 0.247$);

(E3) $k_0 = -0.3414, k_L = -1.852$ (we compute $k_0 k_L = 0.6322$).

In each case, both conditions (16) and (17) for the stability are satisfied.

The evolutions of the water flow at $x = 0$ and of the water level at $x = L$ are depicted at the top of Fig. 10 for these three experiments. The last two graphs contain the evolution of the openings of the gates at $x = 0$ and at $x = L$, respectively, for these three experiments.

In the last experimentations, the speed of the convergence is smaller. For largest gain values of $k_0 k_L$, the closed-loop system starts to oscillate and becomes unstable [consider the experiment (E3)].

The following two remarks can be put into light:

- if the conditions (16) and (17) are satisfied, then we get the stability of the closed-loop system;
- as claimed in Remark 1, the smaller is the product $|k_0 k_L|$, the higher the speed of convergence;

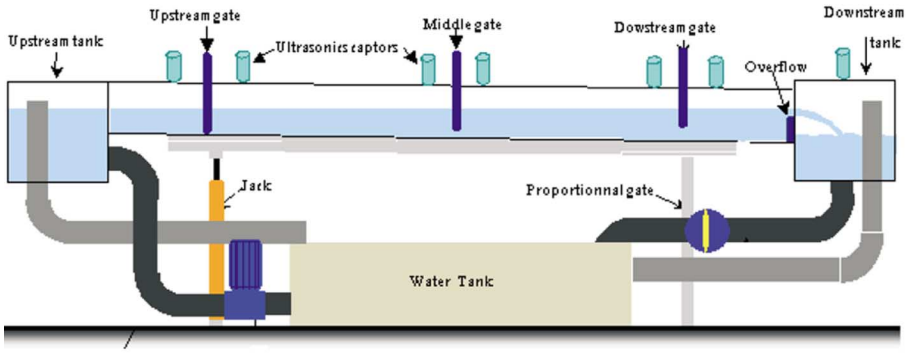

Fig. 8. Pilot channel of Valence.

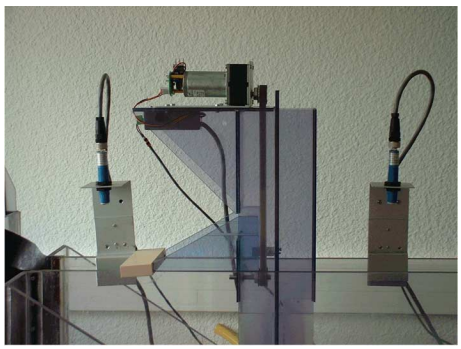

Fig. 9. Pilot channel of Valence: gate and ultrasound sensors.

TABLE II
PARAMETERS OF THE PILOT CHANNEL OF VALENCE

parameters	$B(m)$	$L\ (m)$	$K\ (m^{1/3}.s^{-1})$
values	0.1	7	97
parameters	μ_0	μ_L	slope $(m.m^{-1})$
values	0.6	0.73	1.6 $^0/_{00}$

- to cancel the offset on these experiments, we may add an integral action in a classical manner. See Section V-C for more details.

B. Open-Loop Comparison in the Experiments

Let us compare the convergence speed of the system in closed loop with respect to the one of the open-loop system. On Fig. 11, the same experimentation has been realized in open loop (EOL) at time $t = 130$ s and in closed loop (ECL) at time $t = 70$ s with a parameters product $k_0 k_L = 0.0023$. The arrows in Fig. 11 show that the equilibrium asked is first reached by the closed loop, the open loop takes at least three times more.

C. Adding an Integral Action in the Experiments

To cancel the offset on the experiments, we may add an integral action as in Section IV-D for the numerical simulations.

The system is first in open loop, and at time $t = 50$ s, the control loop is closed. We choose the same initial condition and the same equilibrium as in Section V-A.

To illustrate the effect of the integral action, we select the parameters of the experiment (E2). We recall that, with this choice, the stability condition (16) and (17) is satisfied. Three experiments have been done (see Fig. 12), with the following values.

(EI1) There is no integral action, i.e., $m_0 = 0$ and $m_L = 0$. An offset appears in the water level. This case corresponds to the experiment (E2).

(EI2) Integral coefficients are $m_0 = 0.0005$ and $m_L = -0.0005$. The upstream flow and downstream level converge toward the equilibrium.

(EI3) Integral coefficients are $m_0 = 0.005$ and $m_L = -0.005$. The size of the overshot increases dramatically.

Thus, the integral correction improves the robustness of the control proposed and cancel the offset. The parameters m_0 and m_L should be chosen carefully to avoid an overshot like in (EI3).

VI. CONCLUSION

This paper was concerned with the stability of a hyperbolic system of conservation laws, more precisely, of the nonlinear Saint-Venant equations. A sufficient condition for the stability of the nonhomogeneous system is stated, when the nonhomogeneous part is small in C^1-norm. This criterion is written in terms of the BC and is proven thanks to an analysis of the Riemann coordinates.

This result is illustrated and validated with numerical simulations (using real data) and by experiments for the control of the flow in a reach.

The generalization of this result to other systems of two conservations laws, and also the study of larger hyperbolic system, could be interesting.

APPENDIX

In this Appendix, we prove Theorem 1. To do that, we first need to rewrite the Saint-Venant equations in Riemann coordinates. Due to the lateral flow q, the slope's friction J and the bottom slope I, it gives rise to a system of conservation laws with nonhomogeneous terms (see Appendix A). Then, we will estimate the evolution of the Riemann coordinates along the characteristic curves in Appendix B. This estimation could

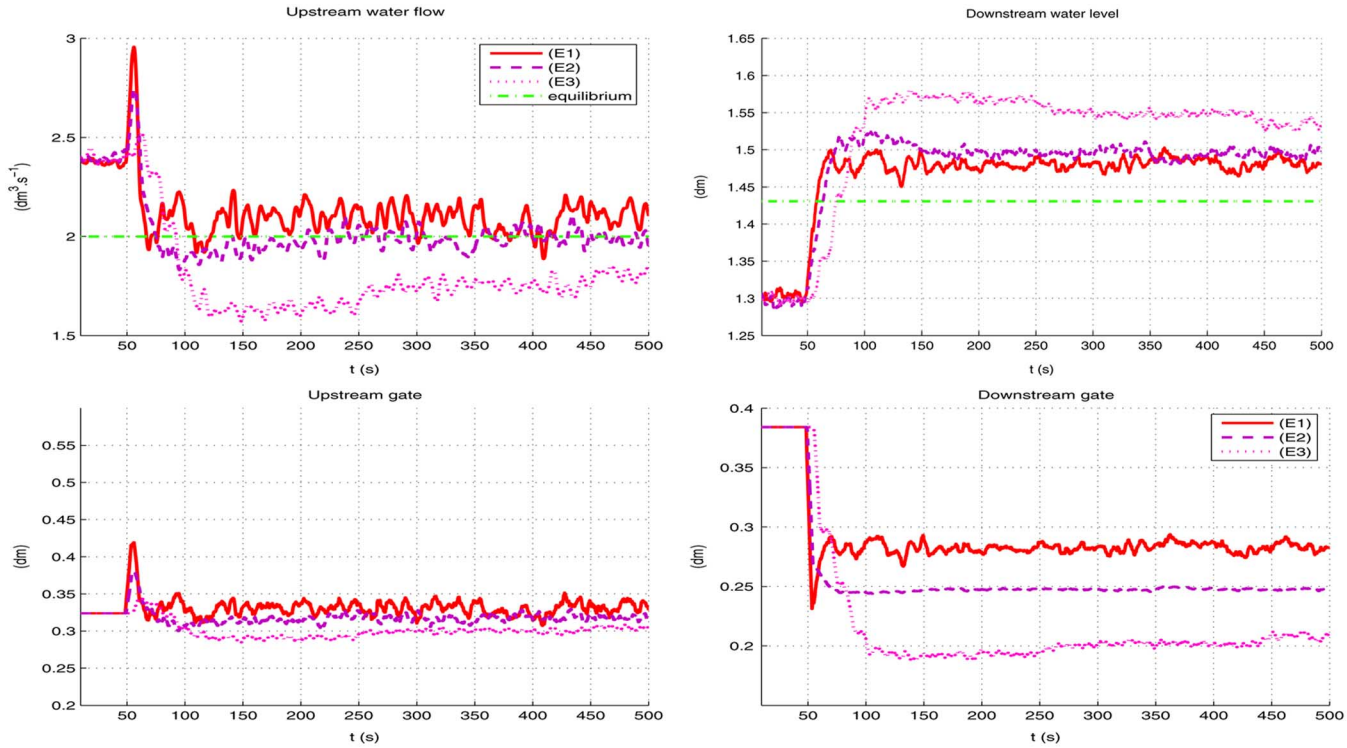

Fig. 10. (Top) Water flow at $x = 0$ and water level at $x = L$ and (bottom) level of the gates at $x = 0$ and $x = L$ for the three experiments (E1)–(E3).

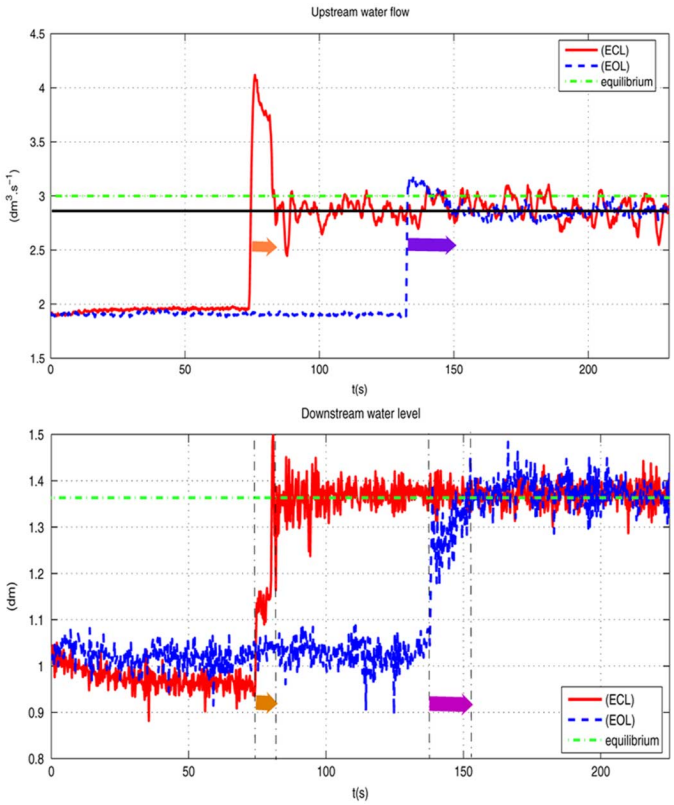

Fig. 11. Water flow at $x = 0$ and water level at $x = L$ for two experimentations (EOL), (ECL).

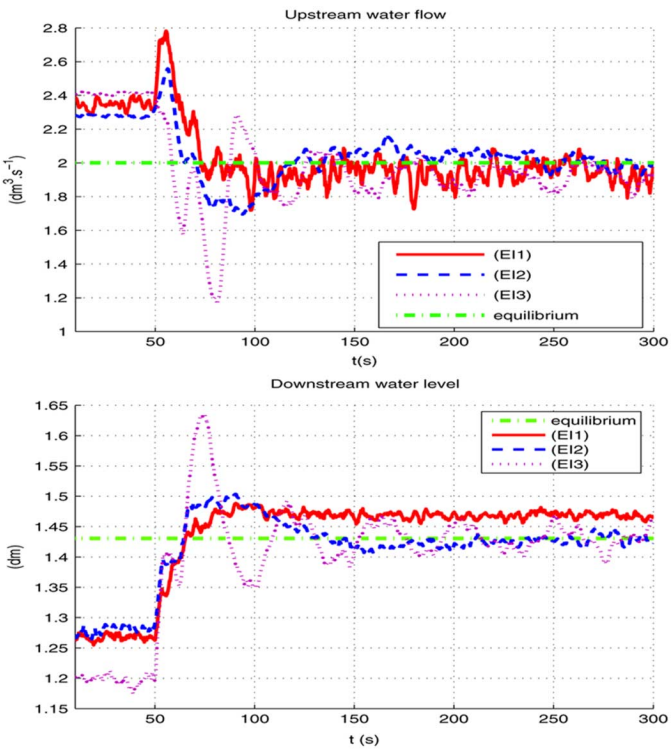

Fig. 12. Water flow at $x = 0$ and water level at $x = L$ for the three experimentations (EI1)–(EI3).

be possible as soon as the nonhomogeneous terms are sufficiently small. These nonhomogeneous terms are estimated in Appendix C. Then, we write a sufficient condition in terms of the BCs for the asymptotic stability of the Riemann coordinates (see Appendix D). This sufficient condition is written as (15).

A. Riemann Coordinates

In this section, we rewrite the PDE (3) in Riemann coordinates. They are defined as follows (see [8]):

$$\xi_1 = \left(\frac{Q}{BH} + 2\sqrt{gH}\right) - \left(\frac{\bar{Q}}{B\bar{H}} + 2\sqrt{g\bar{H}}\right)$$
$$\xi_2 = \left(\frac{Q}{BH} - 2\sqrt{gH}\right) - \left(\frac{\bar{Q}}{B\bar{H}} - 2\sqrt{g\bar{H}}\right).$$

Now the PDE (3) is rewritten as a nonhomogeneous system of conservation laws

$$\partial_t \xi + \Lambda(\xi)\partial_x \xi = h(\xi) \tag{24}$$

where $\Lambda(\xi) = \mathrm{diag}(\lambda_1, \lambda_2)$, and $h(\xi)$ is the nonhomogeneous term. Denoting $h = (h_1, h_2)$, we split h_1 and h_2 into three terms

$$h_1(\xi_1,\xi_2) = \frac{g}{\bar{\lambda}_1}\left[\frac{I}{4}(3\xi_1 + \xi_2) + f_1(\xi_1,\xi_2) + k_1(\xi_1,\xi_2)\right]$$
$$h_2(\xi_1,\xi_2) = \frac{g}{\bar{\lambda}_2}\left[\frac{I}{4}(\xi_1 + 3\xi_2) + f_2(\xi_1,\xi_2) + k_2(\xi_1,\xi_2)\right]. \tag{25}$$

Let us explicit these three terms. To do that, recalling (12), we first note that $\bar{a} \neq \bar{b}$ (indeed if $\bar{a} = \bar{b}$, then $\bar{H} = 0$ which is in contradiction with the fluvial assumption). The first term of the right-hand side of (25) depends only on the slope I. The second one f_i for each $i = 1, 2$ depends only on the friction and is given by

$$f_1(\xi_1,\xi_2) = \frac{n_M^2}{16B^{4/3}}\left[(3\bar{a}+\bar{b})(\xi_1+\xi_2+\bar{a}+\bar{b})^2 \times \left(2 + \frac{16Bg}{(\xi_1-\xi_2+\bar{a}-\bar{b})^2}\right)^{4/3} - (3\xi_1+\xi_2+3\bar{a}+\bar{b})(\bar{a}+\bar{b})^2 \times \left(2+\frac{16Bg}{(\bar{a}-\bar{b})^2}\right)^{4/3}\right]$$
$$f_2(\xi_1,\xi_2) = \frac{n_M^2}{16B^{4/3}}\left[(\bar{a}+3\bar{b})(\xi_1+\xi_2+\bar{a}+\bar{b})^2 \times \left(2 + \frac{16Bg}{(\xi_1-\xi_2+\bar{a}-\bar{b})^2}\right)^{4/3} - (\xi_1+3\xi_2+\bar{a}+3\bar{b})(\bar{a}+\bar{b})^2 \times \left(2+\frac{16Bg}{(\bar{a}-\bar{b})^2}\right)^{4/3}\right].$$

Note that $f_1(0,0) = 0$ and $f_2(0,0) = 0$.

The last terms in (25) are functions of the lateral flow q

$$k_1(\xi_1,\xi_2) = \frac{q}{\bar{\lambda}_1}\frac{g}{B}\left[\frac{(3\bar{a}+\bar{b})}{(\xi_1-\xi_2+\bar{a}-\bar{b})^2} \times \left(\frac{k}{2}(\xi_1+\xi_2+\bar{a}+\bar{b}) - \frac{B}{4}(\xi_1+3\xi_2+\bar{a}+3\bar{b})\right) - \frac{(3\xi_1+\xi_2+3\bar{a}+\bar{b})}{(\bar{a}-\bar{b})^2} \times \left(\frac{k}{2}(\bar{a}+\bar{b}) - \frac{B}{4}(\bar{a}+3\bar{b})\right)\right]$$
$$k_2(\xi_1,\xi_2) = \frac{q}{\bar{\lambda}_2}\frac{g}{B}\left[\frac{(\bar{a}+3\bar{b})}{(\xi_1-\xi_2+\bar{a}-\bar{b})^2} \times \left(\frac{k}{2}(\xi_1+\xi_2+\bar{a}+\bar{b}) - \frac{B}{4}(3\xi_1+\xi_2+3\bar{a}+\bar{b})\right) - \frac{(\xi_1+3\xi_2+\bar{a}+3\bar{b})}{(\bar{a}-\bar{b})^2} \times \left(\frac{k}{2}(\bar{a}+\bar{b}) - \frac{B}{4}(3\bar{a}+\bar{b})\right)\right].$$

Note that $k_1(0,0) = 0$ and $k_2(0,0) = 0$.

We write the BCs (5) and (6) in terms of the Riemann coordinates as follows:

$$\xi_1(t,0) + k_0\xi_2(t,0) = 0 \tag{26}$$
$$\xi_2(t,L) + k_L\xi_1(t,L) = 0 \tag{27}$$

where k_0 and k_L are constant design parameters that have to be tuned to guarantee the stability.

B. Estimation on the Riemann Coordinates

Let us first recall a result of existence (see [3], [9], and [18] for a proof)

Proposition 1: Let $T_2 > T_1 > 0$ and $T = T_2 - T_1$. Assume that the BC satisfies

$$k_0 k_L < 1. \tag{28}$$

Then there exist $\varepsilon(T) > 0, c(T) > 0$ and $H(T)$ such that, for all $\xi^{\#} \in B_{\mathcal{C}}(\varepsilon(T))$ and for all continuously differentiable functions $h : B(\varepsilon(T)) \to \mathbb{R}^n$ such that $h(0) = 0$ holds and

$$|\nabla h(0)| \leq H(T) \tag{29}$$

there exists a unique function $\xi \in C^1([0,L] \times [T_1, T_2], \mathbb{R}^n)$ satisfying the PDE (24) with BCs (26) and (27), and initial condition

$$\xi(x,0) = \xi^{\#}(x) \,\forall x \in [0,L]. \tag{30}$$

Moreover, this function ξ satisfies $\forall t \in [T_1, T_2]$

$$|\xi(.,t)|_{C^0(0,L)} \leq c(T)|\xi^{\#}|_{C^0(0,L)} \tag{31}$$
$$|\xi(.,t)|_{C^1(0,L)} \leq c(T)|\xi^{\#}|_{C^1(0,L)}. \tag{32}$$

Let us estimate the evolution of the Riemann coordinates along the characteristic curves. With the PDE (24) and the BCs (26) and (27), we obtain

$$\begin{aligned}
&\xi_1(L, t_1+t_2)\\
&= \xi_1(0,t_2) + \int_{t_2}^{t_1+t_2} h_1(\xi_1(x(s),s),\xi_2(x(s),s))ds\\
&= -k_0\xi_2(0,t_2) + \int_{t_2}^{t_1+t_2} h_1(\xi_1(x(s),s),\xi_2(x(s),s))ds\\
&= -k_0\left[\xi_2(L,0) + \int_0^{t_2} h_2(\xi_1(x(s),s),\xi_2(x(s),s))ds\right]\\
&\quad + \int_{t_2}^{t_1+t_2} h_1(\xi_1(x(s),s),\xi_2(x(s),s))ds\\
&= k_0k_L\xi_1(L,0) - k_0\int_0^{t_2} h_2(\xi_1(x(s),s),\xi_2(x(s),s))ds\\
&\quad + \int_{t_2}^{t_1+t_2} h_1(\xi_1(x(s),s),\xi_2(x(s),s))ds.
\end{aligned} \tag{33}$$

Thus, we get the estimation

$$|\xi_1(L,t_1+t_2)| \le |k_0k_L||\xi_1(L,0)| + |k_0|.\left|\int_0^{t_2} h_2(\xi_1(x(s),s),\xi_2(x(s),s))ds\right| + \left|\int_{t_2}^{t_1+t_2} h_1(\xi_1(x(s),s),\xi_2(x(s),s))ds\right|.$$

Now, using Proposition 1, if $\varepsilon > 0$ is sufficiently small, then we have

$$|\xi_1(L,t_1+t_2)| \le \{|k_0k_L| + t_2|k_0|.\|\nabla h_2(0)\| + t_1|\nabla h_1(0)| + C(\varepsilon)|\xi^\sharp|_{C^0(0,L)}\} \times |\xi^\sharp|_{C^0(0,L)} \quad (34)$$

where $C(\varepsilon) > 0$ depends only on ε.

To go further into the estimation of the evolution of the Riemann coordinates, we need to compute $|\nabla h|$.

C. Computations of $|\nabla h|$

Denoting $\nabla h(\xi) = \begin{pmatrix} \partial_{\xi_1} h_1(\xi) & \partial_{\xi_2} h_1(\xi) \\ \partial_{\xi_1} h_2(\xi) & \partial_{\xi_2} h_2(\xi) \end{pmatrix}$, we compute similarly the expression of $\partial_{\xi_1} h_1(\xi)$ (given in the equation shown at the bottom of the page). In particular, we have (35), shown at the bottom of the page.

We compute similarly the expression of $\partial_{\xi_2} h_1(\xi)$ (shown in the equation at the bottom of the page). In particular, we have (36), shown at the bottom of the page.

$$\partial_{\xi_1} h_1(\xi) = \frac{g}{\bar\lambda_1}\left\{\frac{3I}{4} + \frac{n_M^2}{16B^{4/3}}\left[2(3\bar a+\bar b)\ (\xi_1+\xi_2+\bar a+\bar b)\left(2+\frac{16Bg}{(\xi_1-\xi_2+\bar a-\bar b)^2}\right)^{4/3} + \frac{4}{3}(3\bar a+\bar b)(\xi_1+\xi_2+\bar a+\bar b)^2 \times\left(-2\frac{16Bg}{(\xi_1-\xi_2+\bar a-\bar b)^3}\right)\times\left(2+\frac{16Bg}{(\xi_1-\xi_2+\bar a-\bar b)^2}\right)^{1/3} - 3(\bar a+\bar b)^2\left(2+\frac{16Bg}{(\bar a-\bar b)^2}\right)^{4/3}\right]\right\} + \frac{q}{\bar\lambda_1}\frac{g}{B}\left[-2\frac{(3\bar a+\bar b)}{(\xi_1-\xi_2+\bar a-\bar b)^3}\left(\frac{k}{2}(\xi_1+\xi_2+\bar a+\bar b) - \frac{B}{4}(\xi_1+3\xi_2+\bar a+3\bar b)\right) + \frac{(3\bar a+\bar b)}{(\xi_1-\xi_2+\bar a-\bar b)^2}\left(\frac{k}{2}-\frac{B}{4}\right) - \frac{3}{(\bar a-\bar b)^2}\left(\frac{k}{2}(\bar a+\bar b) - \frac{B}{4}(\bar a+3\bar b)\right)\right]$$

$$\partial_{\xi_1} h_1(0) = \frac{g}{\bar\lambda_1}\left\{\frac{3I}{4} + \frac{n_M^2}{16B^{4/3}} \times \left[(3\bar a-\bar b)(\bar a+\bar b)\left(2+\frac{16Bg}{(\bar a-\bar b)^2}\right)^{4/3} - \frac{8}{3}16Bg\frac{(3\bar a+\bar b)(\bar a+\bar b)^2}{(\bar a-\bar b)^3}\times\left(2+\frac{16Bg}{(\bar a-\bar b)^2}\right)^{1/3}\right] + \frac{q}{B}\left[-2\frac{(3\bar a+\bar b)}{(\bar a-\bar b)^3}\times\left(\frac{k}{2}(\bar a+\bar b) - \frac{B}{4}(\bar a+3\bar b)\right) + \frac{(3\bar a+\bar b)}{(\bar a-\bar b)^2}\left(\frac{k}{2}-\frac{B}{4}\right) - \frac{3}{(\bar a-\bar b)^2}\left(\frac{k}{2}(\bar a+\bar b) - \frac{B}{4}(\bar a+3\bar b)\right)\right]\right\} \quad (35)$$

$$\partial_{\xi_2} h_1(\xi) = \frac{g}{\bar\lambda_1}\left\{\frac{I}{4} + \frac{n_M^2}{16B^{4/3}} \times \left[2(3\bar a+\bar b)(\xi_1+\xi_2+\bar a+\bar b) \times\left(2+\frac{16Bg}{(\xi_1-\xi_2+\bar a-\bar b)^2}\right)^{4/3} + \frac{4}{3}(3\bar a+\bar b)(\xi_1+\xi_2+\bar a+\bar b)^2 \times\left(2+\frac{16Bg}{(\xi_1-\xi_2+\bar a-\bar b)^3}\right)\left(2+\frac{16Bg}{(\xi_1-\xi_2+\bar a-\bar b)^2}\right)^{1/3} - (\bar a+\bar b)^2\left(2+\frac{16Bg}{(\bar a-\bar b)^2}\right)^{4/3}\right]\right\} + \frac{q}{\bar\lambda_1}\frac{g}{B}\left[2\frac{(3\bar a+\bar b)}{(\xi_1-\xi_2+\bar a-\bar b)^3}\left(\frac{k}{2}(\xi_1+\xi_2+\bar a+\bar b) - \frac{B}{4}(\xi_1+3\xi_2+\bar a+3\bar b)\right) + \frac{(3\bar a+\bar b)}{(\xi_1-\xi_2+\bar a-\bar b)^2}\left(\frac{k}{2}-3\frac{B}{4}\right) - \frac{1}{(\bar a-\bar b)^2}\left(\frac{k}{2}(\bar a+\bar b) - \frac{B}{4}(\bar a+3\bar b)\right)\right]$$

$$\partial_{\xi_2} h_1(0) = \frac{g}{\bar\lambda_1}\left\{\frac{I}{4} + \frac{n_M^2}{16B^{4/3}} \times \left[(5\bar a+\bar b)(\bar a+\bar b)\left(2+\frac{16Bg}{(\bar a-\bar b)^2}\right)^{4/3} + \frac{8}{3}16Bg\frac{(3\bar a+\bar b)(\bar a+\bar b)^2}{(\bar a-\bar b)^3}\times\left(2+\frac{16Bg}{(\bar a-\bar b)^2}\right)^{1/3}\right] + \frac{q}{B}\left[2\frac{(3\bar a+\bar b)}{(\bar a-\bar b)^3}\left(\frac{k}{2}(\bar a+\bar b) - \frac{B}{4}(\bar a+3\bar b)\right) + \frac{(3\bar a+\bar b)}{(\bar a-\bar b)^2}\left(\frac{k}{2}-3\frac{B}{4}\right) - \frac{1}{(\bar a-\bar b)^2}\left(\frac{k}{2}(\bar a+\bar b) - \frac{B}{4}(\bar a+3\bar b)\right)\right]\right\} \quad (36)$$

$$\partial_{\xi_1} h_2(0) = \frac{g}{\bar{\lambda}_2}\left\{\frac{I}{4} + \frac{n_M^2}{16B^{4/3}} \times \left[(\bar{a}+5\bar{b})(\bar{a}+\bar{b})\left(2+\frac{16Bg}{(\bar{a}-\bar{b})^2}\right)^{4/3} - \frac{8}{3}16Bg\frac{(\bar{a}+3\bar{b})(\bar{a}+\bar{b})^2}{(\bar{a}-\bar{b})^3} \times \left(2+\frac{16Bg}{(\bar{a}-\bar{b})^2}\right)^{1/3}\right]\right.$$
$$\left. + \frac{q}{B}\left[-2\frac{(\bar{a}+3\bar{b})}{(\bar{a}-\bar{b})^3}\left(\frac{k}{2}(\bar{a}+\bar{b}) - \frac{B}{4}(3\bar{a}+\bar{b})\right) + \frac{(\bar{a}+3\bar{b})}{(\bar{a}-\bar{b})^2}\left(\frac{k}{2} - 3\frac{B}{4}\right) - \frac{1}{(\bar{a}-\bar{b})^2}\left(\frac{k}{2}(\bar{a}+\bar{b}) - \frac{B}{4}(3\bar{a}+\bar{b})\right)\right]\right\} \quad (37)$$

$$\partial_{\xi_2} h_2(0) = \frac{g}{\bar{\lambda}_2}\left\{\frac{3I}{4} + \frac{n_M^2}{16B^{4/3}} \times \left[-(\bar{a}-3\bar{b})(\bar{a}+\bar{b})\left(2+\frac{16Bg}{(\bar{a}-\bar{b})^2}\right)^{4/3} + \frac{8}{3}16Bg\frac{(\bar{a}+3\bar{b})(\bar{a}+\bar{b})^2}{(\bar{a}-\bar{b})^3} \times \left(2+\frac{16Bg}{(\bar{a}-\bar{b})^2}\right)^{1/3}\right]\right.$$
$$\left. + \frac{q}{B}\left[2\frac{(\bar{a}+3\bar{b})}{(\bar{a}-\bar{b})^3}\left(\frac{k}{2}(\bar{a}+\bar{b}) - \frac{B}{4}(3\bar{a}+\bar{b})\right) + \frac{(\bar{a}+3\bar{b})}{(\bar{a}-\bar{b})^2}\left(\frac{k}{2} - 3\frac{B}{4}\right) - \frac{3}{(\bar{a}-\bar{b})^2}\left(\frac{k}{2}(\bar{a}+\bar{b}) - \frac{B}{4}(3\bar{a}+\bar{b})\right)\right]\right\} \quad (38)$$

In the same way, one obtains for h_2, the expressions (37) and (38), shown at the top of the page, for its partial derivatives.

Using (35)–(38), for all $H > 0$, if the bottom slope function I, the slope's friction function J, and the lateral flow q are sufficiently small in C^1 norm, then $|\nabla h(0)| < H_1$.

D. Conclusion of the Proof of Theorem 1

Coupling (34)–(38), if k_1 and k_2 satisfy (16) and (17), then, we obtain, the existence of a $K, 0 < K < 1$, such that

$$\xi_1(L, t_1 + t_2)| \leq K|\xi^\sharp|_{C^0(0,L)}. \quad (39)$$

This estimate allows a repeated application on intervals of length $\tau = t_1 + t_2$ to give, for all $N \in \mathbb{N} \setminus \{0\}$

$$|\xi_1(L, N\tau)| \leq K^N|\xi^\sharp|_{C^0(0,L)}.$$

A similar condition is obtained when ξ_1 is replaced by ξ_2, and when $x = L$ in (33) is replaced by any $x \in [0, L]$. Thus, by letting $C_1 = e^{-\ln \nu}$ and

$$\mu = -\frac{\ln(K)}{t_1 + t_2} \quad (40)$$

we get

$$|\xi(., t)|_{C^0(0,L)} \leq C_1 e^{-\mu t}|\xi^\#|_{C^0(0,L)} \, \forall t \geq 0.$$

The estimation of $\partial_x \xi$ is obtained in the same way, by differentiating (24) along the characteristics. We get the estimate (22).

We deduce from the BCs (26) and (27), the following conditions:

$$Q_0 = BH_0\left[\frac{\bar{Q}_0}{B\bar{H}_0} - 2\sqrt{g}\alpha_0(\sqrt{H_0} - \sqrt{\bar{H}_0})\right] \quad (41)$$

$$Q_L = BH_L\left[\frac{\bar{Q}_L}{B\bar{H}_L} + 2\sqrt{g}\alpha_L(\sqrt{H_L} - \sqrt{\bar{H}_L})\right] \quad (42)$$

with $\alpha_0 = (1-k_0)/(1+k_0), \alpha_L = (1-k_L)/(1+k_L)$, and k_0 and k_L are the control parameters. From (41) and (42) and the BCs (5) and (6), we deduce (18) and (19).

This concludes the proof of Theorem 1.

Remark 2: Let us note that due to (40), larger is the positive number μ, smaller is the positive number K. Due to (34) and (39), to render the positive number K close to 0, we have to make the product $k_0 k_L$ close to 0. It allows us to estimate the speed of the exponential convergence in Theorem 1 and to prove Remark 1.

ACKNOWLEDGMENT

The authors would like to thank Prof. E. Mendes and the LCIS who have allowed them to carry the experiments on the microchannel.

REFERENCES

[1] S. Cordier, C. Buet, and V. Dos Santos, "A conservative and entropy scheme for a simplified model of granular media," *Transport Theory Stat. Phys.*, vol. 33, no. 2, pp. 125–155, Apr. 2004.

[2] J. M. Coron, B. d'Andréa-Novel, and G. Bastin, "A strict Lyapunov function for boundary control of hyperbolic systems of conservation laws," *IEEE Trans. Autom. Control*, vol. 52, no. 1, pp. 2–11, Jan. 2007.

[3] A. Bressan, *Hyperbolic Systems of Conservation Laws. The One-Dimensional Cauchy Problem*. London, U.K.: Oxford Univ. Press, 2000.

[4] V. Dos Santos, G. Bastin, J.-M. Coron, and B. d'Andréa-Novel, "Boundary control with integral action for hyperbolic systems of conservation laws: Stability and experiments," *Automatica*, to be published.

[5] J.-F. Dulhoste, G. Besançon, and D. Georges, "Nonlinear control of water flow dynamics by input-output linearisation based on a collocation model," presented at the Eur. Control Conf., Porto, Portugal, 2001.

[6] W. H. Graf, *Fluvial Hydraulics*. New York: Wiley, 1998.

[7] J.-M. Greenberg and T.-T. Li, "The effect of boundary damping for the quasilinear wave equations," *J. Diff. Eq.*, vol. 52, pp. 66–75, 1984.

[8] J. de Halleux, C. Prieur, J.-M. Coron, B. d'Andréa-Novel, and G. Bastin, "Boundary feedback control in networks of open channels," *Automatica*, vol. 39, pp. 1365–1376, 2003.

[9] T.-T. Li, "Global Classical Solutions for Quasilinear Hyperbolic Systems," in *Research in Applied Mathematics*. Paris, Milan, Barcelona: Masson and Wiley, 1994.

[10] X. Litrico, V. Fromion, J.-P. Baume, C. Arranja, and M. Rijo, "Experimental validation of a methodology to control irrigation canals based on Saint-Venant equations," *Control Eng. Practice*, vol. 13, pp. 1425–1437, 2005.

[11] X. Litrico and V. Fromion, "H_∞ control of an irrigation canal pool with a mixed control politics," *IEEE Trans. Control Syst. Technol.*, vol. 14, no. 1, pp. 99–101, Jan. 2006.

[12] X. Litrico and D. Georges, "1999, Robust continuous-time and discrete-time flow control of a dam-river system: (I) Modelling," *J. Appl. Math. Model.*, vol. 23, no. 11, pp. 809–827, 1999.

[13] X. Litrico and D. Georges, "1999, Robust continuous-time and discrete-time flow control of a dam-river system: (II) Controller design," *J. Appl. Math. Model.*, vol. 23, no. 11, pp. 829–846, 1999.

[14] P.-O. Malaterre, D. C. Rogers, and J. Schuurmans, "Classification of canal control algorithms," *J. Irrigation Drainage Eng.*, vol. 124, no. 1, pp. 3–10, 1998.

[15] I. M. Y. Mareels, E. Weyer, S. K. Ooi, M. Cantoni, Y. Li, and G. Nair, "Systems engineering for irrigation systems: Successes and challenges," *Ann. Rev. Control*, vol. 29, no. 2, pp. 191–204, 2005.

[16] H. Ouarit, L. Lefevre, and D. Georges, "Robust optimal control of one-reach open channels," presented at the Eur. Control Conf., Cambridge, U.K., 2003.

[17] M. Papageorgiou and A. Messmer, "Flow control of a long river stretch," *Automatica*, vol. 25, no. 2, pp. 177–183, 1989.

[18] C. Prieur, J. Winkin, and G. Bastin, "Robust boundary control of systems of conservation laws," *Math. Control Signal Syst.*, submitted for publication.

[19] E. Weyer, "Decentralised PI controller of an open water channel," presented at the 15th IFAC World Congr., Barcelona, Spain, 2002.

[20] L. Zaccarian, Y. Li, E. Weyer, M. Cantoni, and A. R. Teel, "Anti-windup for marginally stable plants and its application to open water channel control systems," *Control Eng. Pract.*, vol. 15, no. 2, pp. 261–272, 2007.

Valérie Dos Santos was born in Troyes, France, in 1976. She received the M.Sc. degree in mathematics and the Ph.D. degree in applied mathematics from the University of Orléans, Orléans, France, in 2001 and 2004, respectively.

Currently, she is a Professor Assistant with the Laboratory LAGEP, University of Lyon 1, Villeurbanne, France. After one year with the Laboratory of Mathematics MAPMO, Orléans, France, as ATER, she was a Postdoctoral Researcher with the Laboratory CESAME/INMA, the University Catholic of Louvain, Louvain, Belgium. Her current research interests include nonlinear control theory, perturbations theory of operators and semigroup, spectral theory, and control of nonlinear partial differential equations.

Christophe Prieur was born in Essey-les-Nancy, France, in 1974. He received the M.Sc. degree in mathematics from the Ecole Normale Supérieure de Cachan, Cachan, France, in 2000, and the Ph.D. degree in applied mathematics from the Université Paris-Sud, Paris, France, in 2001.

In 2002, he was a Research Associate with CNRS, the Laboratoire SATIE, Ecole Normale Supérieure de Cachan, Cachan, France. Since 2004, he has been with the LAAS-CNRS, Toulouse, France. His current research interests include nonlinear control theory, robust control, and control of nonlinear partial differential equations.